# Automated optimization of microbunching for seeded free-electron laser schemes

Zihan Wang, Zhenghe Bai,[*] Qika Jia,[†] Zhouyu Zhao, and Guangyao Feng[‡]

*National Synchrotron Radiation Laboratory, University of Science and Technology of China, Hefei 230029, China*

(Received 16 January 2026; accepted 28 October 2026; published 10 November 2026)

Seeded free-electron lasers (FELs) have become indispensable tools across numerous scientific fields, owing to their high coherence and stability. Unlike self-amplified spontaneous emission, seeded FELs require a prebunched electron beam to be formed upstream of the radiator, enabling the subsequent generation of fully coherent radiation. This bunching process can be numerically calculated based on the specific components and their parameters used. To facilitate the discovery and optimization of such FELs, in this paper we present an automated optimization method for the microbunching process in seeded FEL schemes. It is demonstrated that the method can automatically reproduce established seeded FELs, such as echo-enabled harmonic generation, eliminating the need for prior physical analysis. Moreover, the method yields new findings in seeded FELs that go beyond mere replication. By incorporating more kinds of components and exploring a broader set of optimization objectives, the optimization can be extended to explore more possibilities.

DOI: 10.1103/bqll-w87s

## I. INTRODUCTION

Free-electron lasers (FELs) represent a transformative light source capable of generating high-brightness, gigawatt-level pulsed beams with femtosecond-scale durations and exceptional spatial-temporal coherence [1–4]. A leading approach to generating x-ray radiation is based on FELs operating in the self-amplified spontaneous emission (SASE) mode [5–8]. However, SASE radiation exhibits limited temporal coherence and pronounced shot-to-shot fluctuations, as the amplification process initiates from stochastic shot noise inherent in the electron beam [9,10]. To overcome these limitations, seeded FELs have been developed as a proven and powerful alternative [11–15]. A seeded FEL operates by imprinting a periodic density modulation onto a relativistic electron beam using external coherent seed lasers and magnetic components. This prebunched beam is then guided into an undulator magnet to initiate the FEL process. Within the high-gain FEL regime, the power is exponentially amplified with the rapid growth of microbunching, producing intense, coherent radiation at the seed wavelength or its harmonics.

[*]Contact author: baizhe@ustc.edu.cn
[†]Contact author: jiaqk@ustc.edu.cn
[‡]Contact author: fenggy@ustc.edu.cn

*Published by the American Physical Society under the terms of the Creative Commons Attribution 4.0 International license. Further distribution of this work must maintain attribution to the author(s) and the published article's title, journal citation, and DOI.*

Within seeded FELs, high-gain harmonic generation (HGHG) [11,13,14,16] is a groundbreaking frequency upconversion scheme that initiates energy modulation with an external seed laser and converts it into density modulation with a chicane. While HGHG can generate the high-order harmonic components of the seed laser frequency, its conversion efficiency decreases markedly with increasing harmonic number. As an alternative seeded FEL scheme capable of operating at high harmonics, echo-enabled harmonic generation (EEHG) [12,15,17–19] employs two seed lasers and two chicanes to generate a much higher harmonic density modulation in the beam from a relatively small initial energy modulation compared to HGHG. Additionally, several seeded FELs introducing more complex transverse-longitudinal coupling phase space manipulation techniques have been proposed to enhance the conversion efficiency, including phase-merging-enhanced harmonic generation (PEHG) [20,21] and angular dispersion-induced microbunching (ADM) [22].

Microbunching formation in the electron beam is crucial for seeded FELs. This process depends solely on the interaction of the electron beam with the seed lasers and the action of the employed magnetic components, without involving the complex dynamics of radiation. Consequently, it can be calculated purely from the functions of the seed lasers and magnetic components, thereby creating a problem of optimizing the layout and parameters of components to form microbunching, which is well-suited for numerical optimization using heuristic algorithms, such as genetic algorithm [23] and particle swarm

algorithm [24]. Therefore, our objective is to develop an automated optimization method for studying the microbunching process in seeded FELs. This method treats the layout and parameters of available components as optimization variables, enabling the automatic generation of optimized seeded FEL configurations for specific performance objectives.

The structure of this paper is as follows. Section II details the automated optimization method for the microbunching process in seeded FEL schemes. Section III A illustrates its application in studying seeded FEL schemes with only two kinds of components, one dedicated to energy modulation and the other to density modulation. Section III B further demonstrates the effectiveness of the optimization method as the number of component types increases. Conclusions and outlook are presented in Sec. IV.

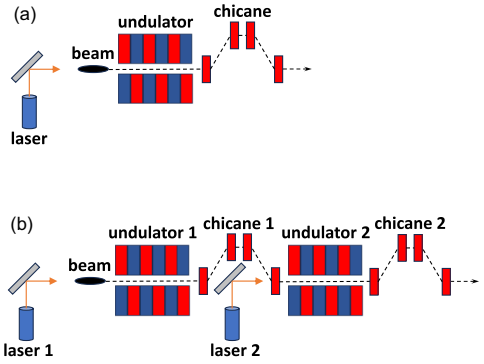



FIG. 1. Schematic layouts of "LC" (a) and "LCLC" (b). In the "LC" layout, HGHG can be achieved, while the "LCLC" layout enables EEHG under optimized component parameters. The dashed lines in both layouts represent the beam path.

## II. METHOD

The distinctions among various seeded FEL schemes stem primarily from differences in the underlying physical principles governing the microbunching process upstream of the radiator. These differences are reflected in the choice of components and their specific parameters. Consequently, different seeded FEL schemes can be simplified using a "black box" model. Within this model, the microbunching process in each scheme is conceptualized as the phase space manipulation of the electron beam achieved through distinct configurations of components.

Consider, for example, a "black box" consisting of $M$ laser-modulators (each comprising a seed laser and a modulator) and $N$ chicanes. We designate a laser-modulator as "L" and a chicane as "C." When $M = 1$ and $N = 1$, the specific sequence "LC" with appropriately optimized parameters has the same microbunching process as the HGHG scheme. Similarly, when $M = 2$ and $N = 2$, the specific sequence "LCLC" with suitably optimized parameters has the same microbunching process as the EEHG scheme. Therefore, HGHG and EEHG can be classified as the "LC" and "LCLC," respectively, as shown in Fig. 1. The two sequences above are only two combinations of "L" and "C." There are other combinations with different numbers and arrangements of "L" and "C," such as "CLLCL." If numerical optimization with heuristic algorithms is applied to such a "black box" model, the optimization process itself can automatically explore among numerous possible configurations and identify the aforementioned two schemes. This would imply that the optimization process possesses the capability to reproduce HGHG and EEHG without prior knowledge of them. This approach also has the potential to discover other seeded FEL schemes that utilize such basic components to achieve optimal microbunching.

The design of seeded FELs typically begins with an analysis of the physical mechanisms responsible for electron beam microbunching. The layout of components and their parameters are optimized through integrating physical theory with mathematical tools. In this work, we propose a numerical optimization approach for achieving microbunching in seeded FELs, where heuristic optimization algorithms such as multiobjective genetic algorithms (MOGAs) [23,25,26] are employed. First, we set up the "black box" model, treating the configuration of basic components, which includes their combination and parameters, as a set of optimization variables. For each configuration solution with a given initial electron beam, the optimization objectives, such as the bunching factor and energy spread, are calculated by analyzing the phase space at the exit of the configuration. The use of MOGA enables the search for optimal seeded FEL schemes by iteratively evaluating and comparing the configuration solutions, thereby efficiently identifying high-performance schemes within the solution space defined by the "black box" model. In this work, MOGA is employed as a representative optimization algorithm, and other multiobjective optimization algorithms can also be used.

This leads to an automated optimization method for the critical microbunching process in seeded FELs. The schematic structure and workflow of the proposed optimization method are illustrated in Fig. 2. For clarity, the optimization is organized into five functional modules: (i) the component definition module, (ii) the initial beam state, (iii) the final beam state, (iv) the objective function module, and (v) the "black box" module. The component definition module specifies the components applicable to seeded FELs, such as seed lasers and chicanes. Their layouts and parameters are treated as optimization variables, and each set of variables constitutes a configuration solution. The initial beam state defines the parameters of the initial electron beam, including beam energy, relative energy spread, and phase space distribution. The final beam state characterizes the beam properties at the exit of the configuration, which represent the unique signature of each configuration solution. The objective function

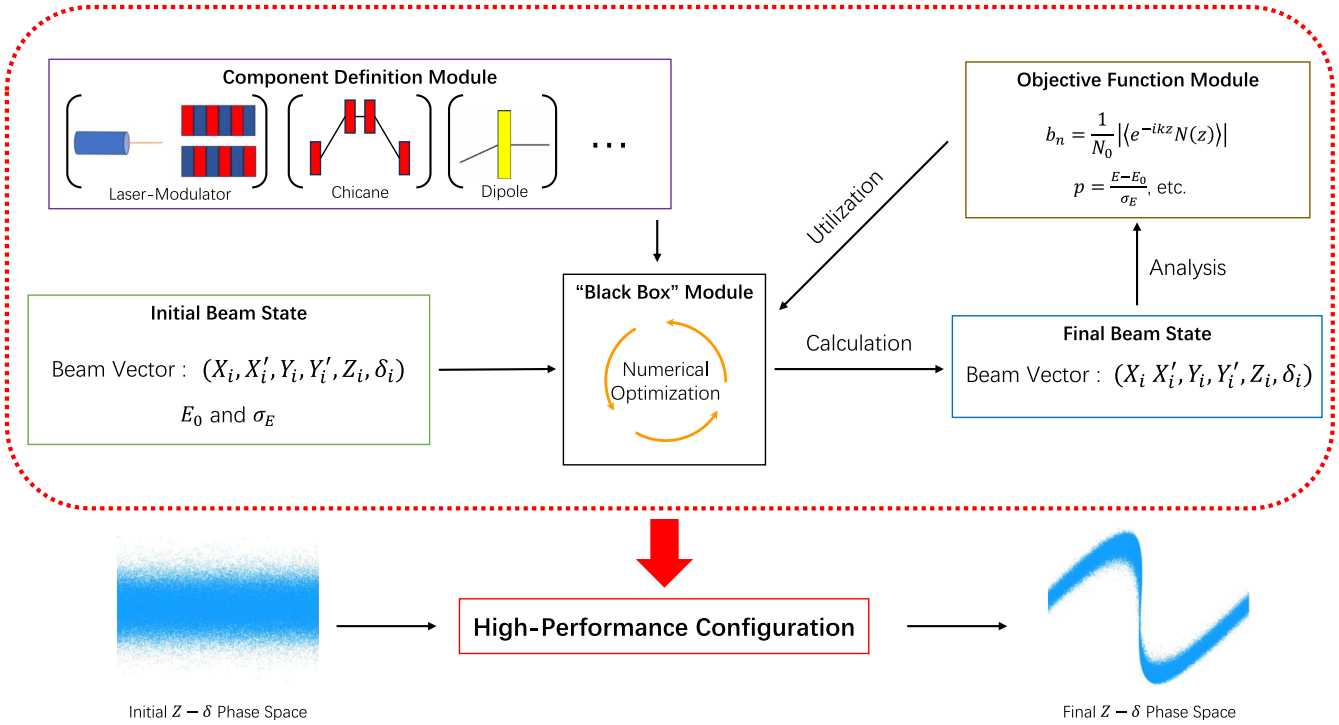



FIG. 2. The schematic structure and workflow of the automated optimization method for the microbunching process in seeded FELs. First, each layout constructed using components from the component definition module and beam parameters from the initial beam state, serving as the initial conditions, are passed to the "black box" module for numerical optimization with heuristic algorithms. Within the "black box" module, potential seeded FEL configurations are simulated to calculate the evolution of beam state. For each configuration solution, the resulting beam information is the final beam state at the exit of the configuration. This information is analyzed based on the given objective functions, and the candidate solutions are sorted into distinct nondominated layers. The ranking results are then utilized to guide the next cycle of numerical optimization. Through multiple iterations of this process, the method ultimately generates high-performance seeded FEL configurations optimized with specified objectives.

module defines the performance metrics of microbunching, which are optimized using heuristic algorithms like MOGA. Finally, the "black box" module performs numerical optimization with heuristic algorithms, utilizing the components from the component definition module and the initial beam parameters to generate seeded FEL configurations with optimal microbunching.

The proposed method enables automated analysis and generation of seeded FEL schemes. It not only identifies optimal configurations but also assists in the study of microbunching formation, thereby extending the knowledge of physical mechanisms involved in the microbunching process in seeded FELs. Moreover, the established modules are designed to be modifiable and extensible according to the physical problem under consideration.

## III. APPLICATION

### A. Example I: Seeded FEL configurations with laser-modulators and chicanes

We first demonstrate the optimization method with a simple example, where we aim to identify high-performance seeded FEL configurations composed solely of laser-modulators for energy modulation and chicanes for density modulation. The study of this paper does not consider the specific treatment of the last radiator in seeded FELs, as it does not affect the microbunching process. Considering the synchronization challenges inherent in multilaser systems and the complexity of configuration, we limited the constituents of the component definition module to three laser-modulators and three chicanes. Each laser-modulator provides standard sinusoidal energy modulation.

We adopt standard FEL parameters for the initial beam state, characterized by an initial Gaussian energy distribution with an average energy of 1.2 GeV and a rms energy spread of 0.15 MeV. Following the notation in Ref. [18], we use the variable $z$ for the longitudinal coordinate in the beam and $p = (E - E_0)/\sigma_E$ for the dimensionless energy deviation of a particle, where $E_0$ is the average energy and $\sigma_E$ is the rms energy spread. Then, the initial longitudinal phase space distribution can be written as $f_0(p) = N_0 e^{-p^2/2}/\sqrt{2\pi}$, where $N_0$ is the total number of electrons per unit length within the beam slice. In this example, we define the unit length as 100 μm and $N_0 = 25000$. It is noted that the value of $N_0$ is significantly

smaller than those in actual seeded FELs. In our optimization, it is necessary to compute the beam evolution across numerous configurations, so this value was chosen to manage the computational cost. As a result, the optimized parameter values under this simplified condition may not represent the true optimum for a realistic seeded FEL model, and absolute quantities such as the bunching factor may also deviate from those in practical setups. Nevertheless, we have confirmed through verification simulations using 2.5 million electrons that this parameter choice adequately captures the essential physical processes governing the formation and evolution of microbunching. Thus, it remains suitable for qualitative studies and for elucidating the underlying physical mechanisms.

We approximate that the longitudinal coordinate of each electron in the beam remains unchanged when passing through the laser-modulator. The beam energy deviation $p'$ after the laser-modulator is given by

$$p' = p + (\Delta E/\sigma_E)\sin(k_s z + \varphi), \tag{1}$$

where $\Delta E$ is the amplitude (modulation strength), $k_s$ is the wave number, and $\varphi$ is the phase. The longitudinal coordinate change for each electron is described by

$$z' = z + R_{56} p \sigma_E / E_0, \tag{2}$$

where $R_{56}$ is the dispersive strength. Table I lists the ranges of the parameters for the laser-modulators and chicanes used in the optimization.

#### 1. Optimization of harmonic number and bunching factor

To achieve a shorter-wavelength fully coherent FEL, it is necessary to maximize the harmonic number while maintaining longitudinal coherence. An important parameter for assessing longitudinal coherence is the bunching factor, which is defined at the wave number $k$ as

$$b = \frac{1}{N_0}|\langle e^{-ikz} N(z)\rangle|, \tag{3}$$

where $N(z) = \int_{-\infty}^{\infty} f(z,p)dp$ defines the beam density as a function of $z$, with $f(z,p)$ being the distribution function, and $\langle\cdots\rangle$ represents taking the average of the function within the brackets per unit length.

TABLE I. Component parameter ranges for Example I.

| Parameter[a] | Min. value | Max. value | Unit |
|---|---|---|---|
| Wavelength (L) | 160 | 360 | nm |
| Modulation strength (L) | 0.0075 | 1.5 | MeV |
| Phase (L) | $-\pi$ | $\pi$ | rad |
| Dispersive strength (C) | 0 | 0.1 | m |

Abbreviations: L = laser; C = chicane.

For the MOGA used in the method, we employ the widely used nondominated sorting genetic algorithm II (NSGA-II) [23]. NSGA-II is used as one example of an optimization algorithm, and it can be replaced by other high-performance optimization algorithms without changing the overall optimization workflow. The harmonic number and bunching factor are designated as the two optimization objectives for each individual that represents a seeded FEL configuration solution. In the application of NSGA-II to our optimization problem, some issues are addressed as follows.

(i) Criterion of configuration comparison: For a specific seeded FEL configuration, its bunching factor varies at different harmonic numbers. Since the bunching factor is generally larger at lower harmonics, simply optimizing for the peak bunching factor tends to make the population converge toward low harmonics. To avoid this, a representative harmonic number and the corresponding bunching factor are selected for each individual according to the following rule. First, for each harmonic number $n(n = 1, 2, \ldots, 200)$, the maximum bunching factor $b_n^{\max}$ across the current population is determined. Then, for each individual, the harmonic number at which its bunching factor is closest to $b_n^{\max}$ is used. If this condition is satisfied for multiple harmonic numbers, the largest harmonic number is used. By grouping individuals by their assigned harmonic numbers and comparing their bunching factors within each group, the population is guided to develop across a wide range of harmonics. Additionally, a precedence rule is applied to favor individuals with fewer components. For any two individuals $i$ and $j$ with the same harmonic number $n$, if the absolute difference of their bunching factors $|b_{n,i} - b_{n,j}| < \Delta_{ij} \cdot \tau(n)$, then the one with fewer components is ranked higher, where $\Delta_{ij}$ represents the difference in the number of components used in $i$ and $j$, and $\tau(n)$ is a scaling factor that depends on the harmonic number $n$. The scaling factor $\tau(n)$ should be positive and nonincreasing with respect to $n$. In this paper, we set

$$\tau(n) = \begin{cases} 0.125, & n \leqslant 8, \\ 1/n, & n \geqslant 9. \end{cases} \tag{4}$$

(ii) Coarse-to-fine optimization strategy: In principle, the harmonic number and bunching factor can be optimized over all possible component layouts. However, the initial sub-population size for each layout is often constrained by computational hardware limitations, which can cause the optimization to converge to local optima. In addition, for complex layouts, individuals exhibiting poor initial performance can impair evolution efficiency, risking premature elimination, and the loss of optimal configurations. To address this issue, we adopt the following coarse-to-fine optimization strategy. First, all possible layouts are divided into some groups based on their structural complexity, and a coarse-grained optimization is performed in

each group to search for promising candidate layouts. Then, a subsequent fine-grained optimization is conducted for each promising layout using a separate run of the NSGA-II algorithm to optimize the harmonic number and bunching factor. The separate optimization of each layout results in a Pareto-optimal solution set, and subsequently, all such sets are merged into a total solution set. Finally, the optimal seeded FEL configuration for each harmonic number is determined by comparing the total set. This coarse-to-fine optimization strategy allows each promising layout to be optimized independently and deeply, preventing premature competition and thereby greatly increasing the likelihood of finding global optima for complex layouts.

(iii) Postprocessing selection: Due to the inherent randomness and nonexhaustive exploration of the NSGA-II algorithm, not every layout yields the optimal solution at all harmonic numbers. For instance, the "LCLC" layout proves to be optimal at the 52nd, 53rd, 55th, and 56th harmonics, but its Pareto front lacks a feasible solution at the 54th harmonic. This does not imply that the "LCLC" layout is physically infeasible for the 54th harmonic. Rather, the algorithm fails to find such a solution due to the complexity of the optimization problem. Among the layouts that did yield feasible solutions at this harmonic, the "LCLLC" layout exhibits the best performance. However, by interpolating the bunching factors for the "LCLC" layout from neighboring harmonics, an estimated solution for the 54th harmonic can be derived, which theoretically dominates the solution found with the "LCLLC" layout. This indicates that the "best" performance of the "LCLLC" layout at the 54th harmonic does not reflect a real "optimal" solution. To filter out such spurious "optimal" solutions, we performed a postprocessing selection via interpolation and performance comparison within different harmonic number regions.

There are also two points worth mentioning. First, the crossover and mutation operators are adapted, where the component layout of each individual is unchanged and its component parameters are varied. For example, an individual with the "LCLC" layout undergoes crossover only with another individual that also has the "LCLC" layout. Second, to reduce computational cost, we excluded two categories of impractical layouts before optimization: those without laser-modulator, and those placing it at the end. In addition, since a single chicane with a large $R_{56}$ can represent the function of consecutive chicanes, the consecutive chicanes in a layout were consolidated into a single chicane with $R_{56}$ in a large range. After the coarse-grained optimization, five promising layouts were identified: "LC," "LLC," "LCLC," "LCLLC," and "LCLCLC."

The final solutions are presented in Fig. 3, which exhibit four layouts. The "LLC" layout was dominated by other layouts. Since the coarse-to-fine optimization strategy could also theoretically carry a risk of missing the global optima, a comparative experiment was conducted by performing a detailed optimization over the entire solution space. The optimization results are very similar to those obtained with the coarse-to-fine strategy, confirming that the strategy is reliable in practice. It is noteworthy that in the figure, within each optimized solution containing $\geqslant 2$ laser-modulators, the employed laser wavelengths are very similar, though the laser wavelengths differ across different solutions. This implies that, in principle, a seeded FEL configuration can be realized based on a single laser source, followed by beam splitting, phase control, and individual amplification. The code used in this example is publicly available on Zenodo [27].

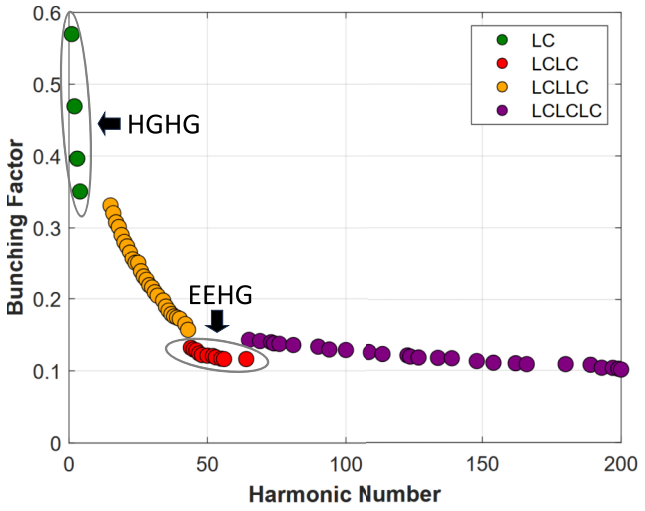



FIG. 3. Harmonic numbers and bunching factors of optimized results with different component layouts. The "LC" denotes a layout beginning with a laser-modulator followed by a chicane, and similar naming applies to other layouts. The optimized results corresponding to HGHG and EEHG are marked in the figure.

For the optimization results shown in Fig. 3, we now explain the physics behind the transition points where the optimal layout changes. The optimized solutions corresponding to the green dots, which are the well-known HGHG schemes, generate significant microbunching in the vicinity of the fundamental frequency. Figure 4(a) presents the final longitudinal phase space distribution obtained with the optimized solution at the 4th harmonic. In the optimization, the maximum energy modulation strength was set to 10 times the rms beam energy spread. Consequently, the bunching factor of the optimized configurations with the "LC" layout decays rapidly for harmonic numbers exceeding 10. For harmonic numbers between 10 and 40, the "LCLLC" layout outperforms the "LCLC" layout corresponding to the EEHG scheme. The reason is that the "LCLLC" layout enables a higher modulation strength in the second energy modulation stage, which is crucial for achieving a large bunching factor. However, as the harmonic number increases, the required energy modulation strength exceeds the upper

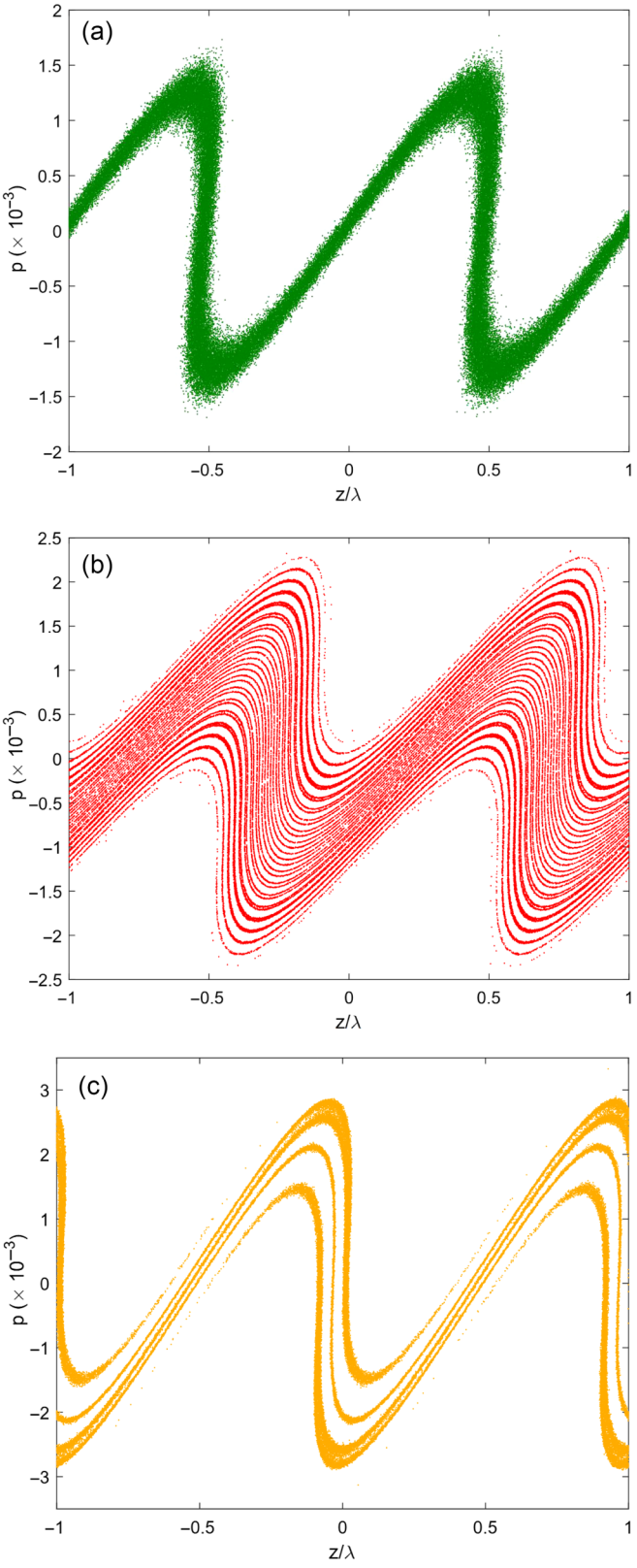



FIG. 4. Final longitudinal phase space distributions of the optimized solutions at the 4th (a), 50th (b), and 20th (c) harmonics, corresponding to the "LC," "LCLC," and "LCLLC" layouts, respectively.

limit that the "LCLLC" layout can provide, leading to a gradual degradation in its performance. In the regime with higher harmonic numbers, the "LCLC" layout becomes more advantageous with fewer components.

Specifically, Fig. 4(b) shows the final phase space distribution of the optimized solution at the 50th harmonic with the "LCLC" layout, and Fig. 4(c) displays that at the 20th harmonic with the "LCLLC" layout. It is seen that the optimized solutions utilizing the "LCLLC" layout represent a new seeded FEL scheme, which is different from HGHG and EEHG. In fact, a similar effect can also be produced by the "LCLC" layout, where the second energy modulation strength is much stronger than that of EEHG. Notably, although the "LLCLC" and "LCLLC" layouts are very similar, the "LLCLC" is not a promising layout. This is because, for the new scheme, the required modulation strength in the second energy modulation stage is larger than that in the first stage. Consequently, placing an additional laser-modulator at the second location is more effective than placing it at the first location. The details for this new scheme will be presented in the next two subsections.

Additionally, an FEL scheme with three modulation stages is also presented in Fig. 3, where each stage consists of a laser-modulator followed by a chicane. Its schematic structure with the "LCLCLC" layout is depicted in Fig. 5. Although the "LCLCLC" layout is the most complex, it is considered the best for very high harmonics, with a bunching factor of approximately 0.1 reached even at the 200th harmonic. Figure 6 illustrates the evolution of the longitudinal phase space obtained with the optimized solution at the 100th harmonic. As depicted, the phase space transformation in the second and third stages is similar to that in the EEHG scheme. The key difference lies in the introduction of an additional initial modulation stage, which induces a prebunching beam, as shown in Fig. 6(b), instead of the initial Gaussian beam in the EEHG scheme. To achieve a large bunching factor at a very large harmonic (e.g., the 100th harmonic), the EEHG scheme requires a rather large energy modulation amplitude in the first modulator, which inherently dilutes the electron density around the reference energy, resulting in a nonuniform distribution in energy stripes. This is addressed in the first modulation stage of the "LCLCLC" scheme by imprinting a periodic density structure. Consequently, the final current distribution is more uniform than that of

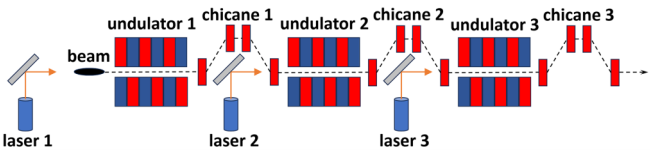



FIG. 5. Schematic layout of the "LCLCLC" scheme. The dashed line represents the path of the beam.

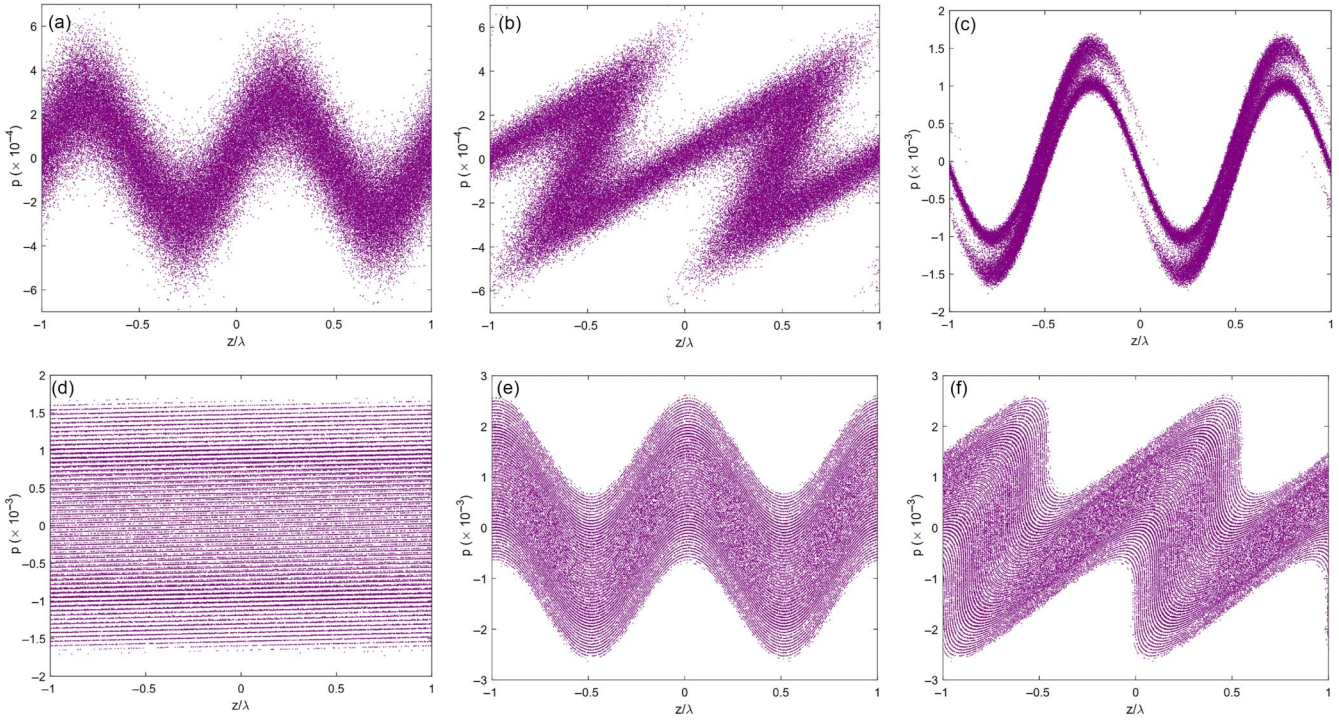



FIG. 6. Longitudinal phase space evolution at the exits of the first modulator (a), first chicane (b), second modulator (c), second chicane (d), third modulator (e), and third chicane (f) in the "LCLCLC" scheme, obtained with the optimized solution at the 100th harmonic.

EEHG, as illustrated in Fig. 7, which leads to a larger bunching factor at a very large harmonic.

### 2. *Optimization of bunching factor and energy spread for specific harmonics*

In the optimization above, the final beam energy spread was not considered. A large energy spread will degrade the performance of the subsequent lasing process. Therefore, next we will simultaneously maximize the bunching factor at a specific harmonic and minimize the final energy spread using the optimization method. For the final energy spread, we use the ratio of the final energy spread to the initial one as an optimization objective. The five promising component layouts mentioned in the previous subsection were investigated separately, and for each layout, four optimizations were performed for the 6th, 15th, 30th, and 60th harmonics. Figure 8 shows the optimized Pareto fronts for these layouts, where results with the same harmonic are combined in a single plot.

In Fig. 8, the optimized solutions with the simple "LC" layout, corresponding to HGHG, have significantly larger final energy spread, which grows substantially as the harmonic number increases. The "LLC" layout with an extra laser-modulator performs similarly to the "LC" layout but yields a larger bunching factor due to the broader modulation range provided by its two seed lasers. In contrast, the "LCLC" layout can achieve a considerably large bunching factor at the same final energy spread, which becomes pronounced at higher harmonics. Similarly, the "LCLLC" layout with an extra laser-modulator exhibits comparable performance to "LCLC," but has a wider Pareto front. This wider Pareto front stems from the two consecutive laser-modulators at the second modulation stage, whereas adding an extra laser-modulator at the first stage provides no benefit. For the "LCLCLC" layout, it can provide a further reduction in energy spread at the same bunching factor. However, this improvement is less significant than that achieved from "LC" to "LCLC." This indicates that further addition of laser-modulators and chicanes may offer little reduction in energy spread and thus only limited gains in radiation performance, at the cost of significantly increased configuration complexity.

Furthermore, we identify a seeded FEL scheme different from EEHG with the same layout, which was mentioned in the previous subsection. In Fig. 8, a notable inflection point appears in each plot, as indicated by the black arrow. Analysis of the phase space evolution reveals that EEHG occurs below the inflection point, while the new scheme occurs above it, with higher energy spread and larger bunching factor. In addition, the final energy spread at the inflection point increases with the harmonic number. In Fig. 8(d) for the 60th harmonic case, the new scheme is presented with the "LCLLC" layout instead of the "LCLC" layout, due to the limited modulation strength of the seed laser. Given the similarity between the optimized solutions with the "LCLLC" and "LCLC" layouts, it is predicted that

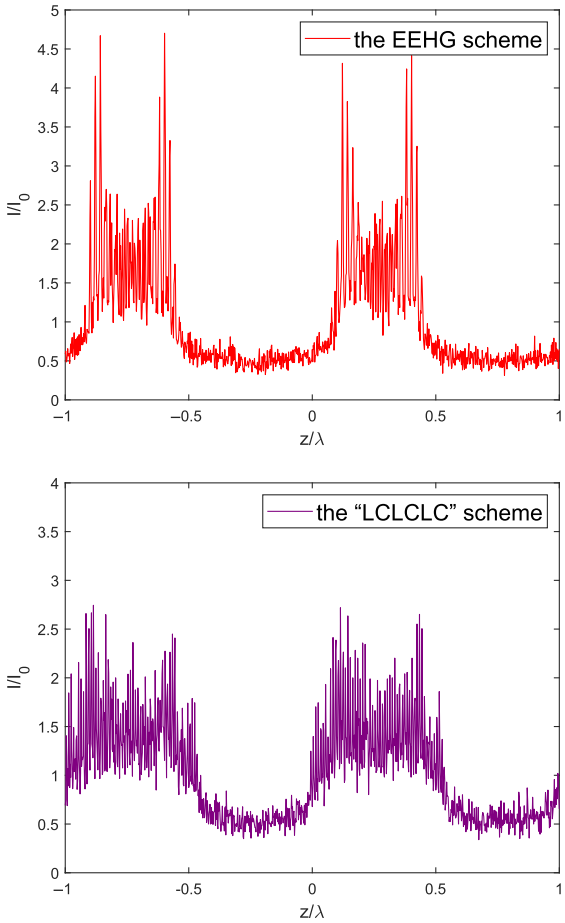



FIG. 7. Comparison of the final current distributions for the EEHG scheme (top) and the "LCLCLC" scheme (bottom), obtained with the optimized solutions at the 50th and 100th harmonics, respectively.

the new scheme can also be realized using the "LCLC" layout with a higher modulation strength. Figure 9 compares the longitudinal phase spaces at different locations of the EEHG and new schemes for two optimized solutions in Fig. 8(c). It is clearly seen that the final phase space distribution of the new scheme differs from the stripe structure of EEHG, although both schemes use the "LCLC" layout. The bunching factors of these two optimized solutions with the EEHG and new schemes are shown in Fig. 10.

In the EEHG scheme, the electron beam first passes through a laser-modulator and a chicane, forming energy stripes. A second seed laser then imprints a fine modulation on the stripes. Typically, the energy modulation induced by the first seed laser is significantly stronger than that of the second. In contrast, the new scheme relies on a strong energy modulation induced by the second seed laser as the key to generating microbunching. Consequently, the strength of the second energy modulation exceeds that of the first one. Furthermore, the required $R_{56}$ value of the first chicane in this new scheme is substantially smaller than that of the EEHG scheme, as is evident from comparing Figs. 9(a) and 9(d). The theoretical maximum bunching factor at the $n$th harmonic for EEHG is approximately $0.39/(n+1)^{1/3}$ [18], while the new scheme is free from this constraint, which can be observed from Fig. 8. Compared with HGHG, it achieves lower final energy spread and larger bunching factor.

To validate the ability of the automated optimization method to correctly identify seeded FELs, we compared the theoretical and optimized values of the component parameters for HGHG at the 6th harmonic: the seed laser modulation strength ($\Delta E$), the seed laser wave number ($k_s$), and the chicane dispersive strength ($R_{56}$). As illustrated in Fig. 11, the optimized parameter values (red dots) approach the theoretical values as the modulation strength increases, with a discrepancy at low modulation strengths due to the influence of the initial energy spread on the selection of optimal parameter values. To verify this influence, we only reduced the initial energy spread from 150 to 15 keV and optimized the "LC" layout for the 6th harmonic. The optimized solutions, represented as green dots in Fig. 11, show very good agreement with the theoretical prediction, confirming the reliability of the optimization method.

### 3. Analysis of the new scheme with the "LCLC" layout

In the two optimizations above, numerical simulations with a radiator were not performed due to the potentially large number of configurations. To demonstrate the FEL performance of the optimization results, we take the new scheme with the "LCLC" layout as an example and analyze its performance under realistic accelerator and beam conditions, including typical errors and collective effects. We use the parameters of the optimized solution at the 30th harmonic that correspond to the new scheme in Figs. 9 and 10.

The simulation was carried out using the time-dependent mode of GENESIS [28] and took into account shot-by-shot variations. The beam energy and rms energy spread are the same as those in the optimization above. The peak current is 800 A, and the normalized emittance is 1 mm rad. The radiator has six sections, each 2.5 m long, with a period length of 5 cm. There are six drifts of 0.5 m for focusing, five between the sections and one at the end. Figure 12 shows the simulated FEL performance. In the top plot, the new scheme exhibits rapid power growth in the early stage due to its large bunching factor and reaches a peak power exceeding 500 MW at the exit of the radiator. In the bottom plot, the spectrum indicates that the bandwidth of the radiation is close to the Fourier-transform-limited.

For typical errors, we investigated the sensitivity of the bunching factor to fluctuations of the seed laser powers within $\pm 5\%$ and magnetic fields of the chicanes within $\pm 0.1\%$ by introducing random variations over 1000 trials.

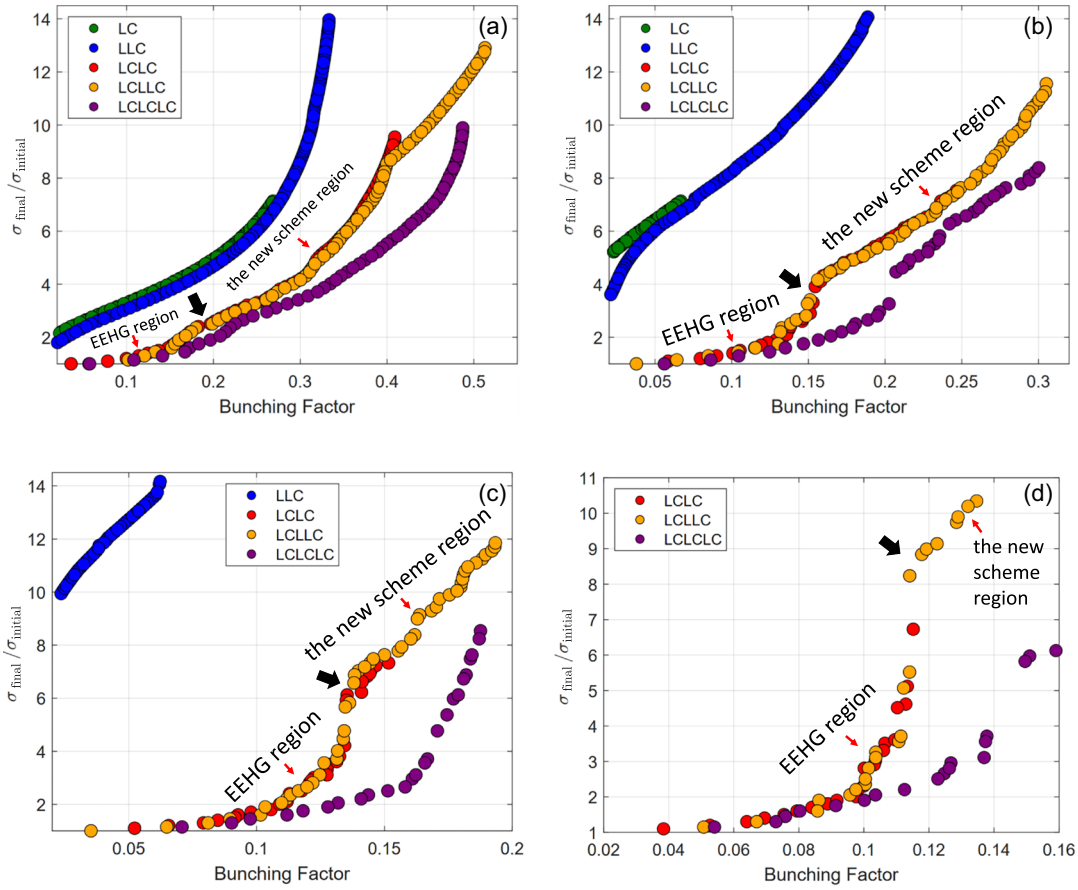



FIG. 8. Comparison of $\sigma_{\text{final}}/\sigma_{\text{initial}}$ and bunching factor for the optimized solutions with different layouts, where $\sigma_{\text{final}}/\sigma_{\text{initial}}$ is the ratio of the final beam energy spread to the initial one. The solutions were optimized at the 6th (a), 15th (b), 30th (c), and 60th (d) harmonics. The position indicated by the black arrow in each plot is the inflection point representing the boundary between EEHG and the new scheme. The regions corresponding to EEHG and the new scheme are further indicated in each plot using text labels and red arrows.

The resulting fluctuations of the bunching factor at the 30th harmonic are shown in Fig. 13. In the absence of errors, the bunching factor is 0.123. When errors are considered, its average value is 0.115, with the bunching factor exceeding 0.1 in most cases, demonstrating the stability of the new scheme.

We also analyzed collective effects, including coherent synchrotron radiation (CSR) and space charge. For the CSR effect in the chicanes, the required value of the first $R_{56}$ of the new scheme is an order of magnitude smaller than that of EEHG, and the second $R_{56}$ of the new scheme is also substantially smaller than that of EEHG. Therefore, the CSR effect in the new scheme should be very weak. An analysis similar to that in Ref. [18] also confirmed that the CSR effect of the new scheme can be neglected. The space charge effect has an impact on the radiation power. Simulations show that after an 18-m-long radiator, the peak power decreases by about 60% compared to the case without considering the space charge effect. However, in the first half of the radiator, the reduction in radiation power is very small. This observation suggests that, by taking advantage of the large bunching factor of the new scheme, a shorter radiator of about 8 m can be employed. In this case, the influence of the space charge effect is very weak, and a peak radiation power of approximately 100 MW is achieved.

The proposed optimization method does not account for variations in the initial beam distribution and errors, as incorporating them would hinder convergence and demand significant computational resources due to the large number of candidate solutions. An efficient search for seeded FEL schemes can be achieved by first performing an error-free optimization and then verifying the optimization results with errors included.

### B. Example II: Seeded FEL configurations with more kinds of components

In the optimizations above, only two kinds of components were applicable. To enrich the component definition module in the optimization method, we therefore added components that can introduce transverse-longitudinal coupling, which has been applied in studying seeded

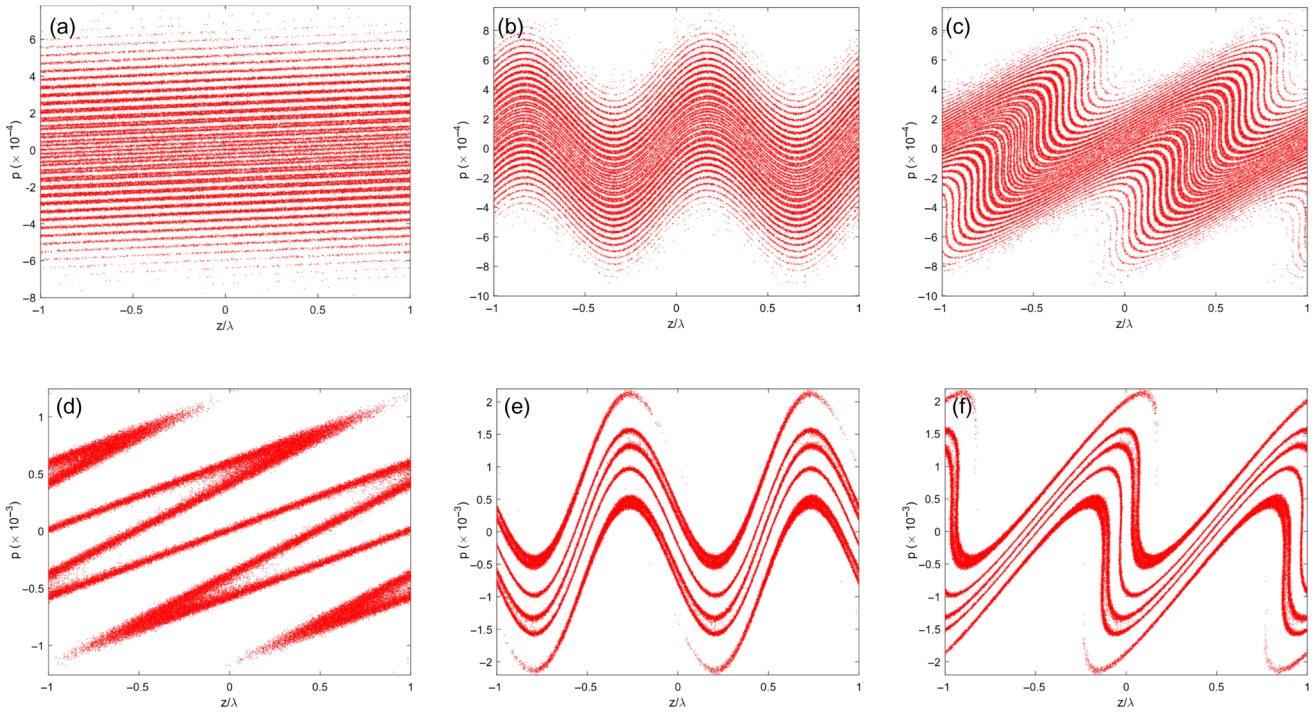



FIG. 9. Comparison of longitudinal phase space evolutions of EEHG and the new scheme for two optimized solutions at the 30th harmonic. The three top plots are the longitudinal phase space distributions at the exits of the first chicane (a), the second laser-modulator (b), and the second chicane (c) in the EEHG scheme. The three bottom plots are the longitudinal phase space distributions at the exits of the first chicane (d), the second laser-modulator (e), and the second chicane (f) in the new scheme.

FEL schemes [20–22,29–32]. The seeded FELs utilizing transverse-longitudinal coupling require ultralow transverse emittances. Since the vertical emittances of low-emittance storage ring light sources can satisfy this requirement, we used the beam parameters of the Hefei Advanced Light Facility (HALF) storage ring [33] for the initial beam, which are listed in Table II. A vertical emittance of 10 pm rad is adopted, considering the suppression of the severe intrabeam scattering effect. The unit length and $N_0$ for the initial beam are the same as in Example I.

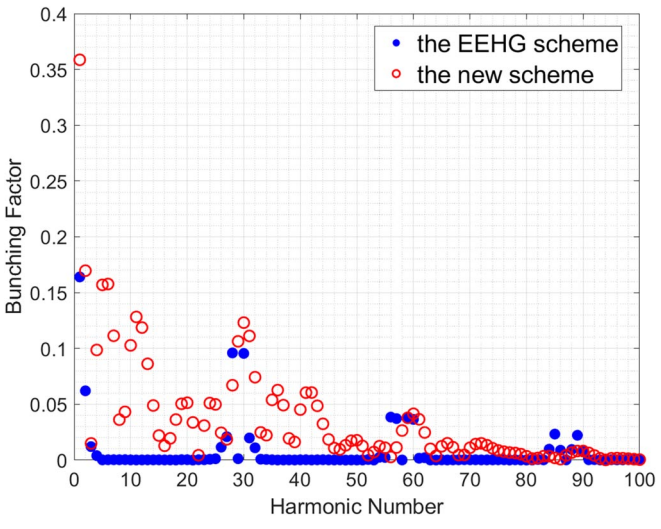



FIG. 10. Comparison of the bunching factors of EEHG (blue dots) and the new scheme (red circles) for two solutions optimized at the 30th harmonic.

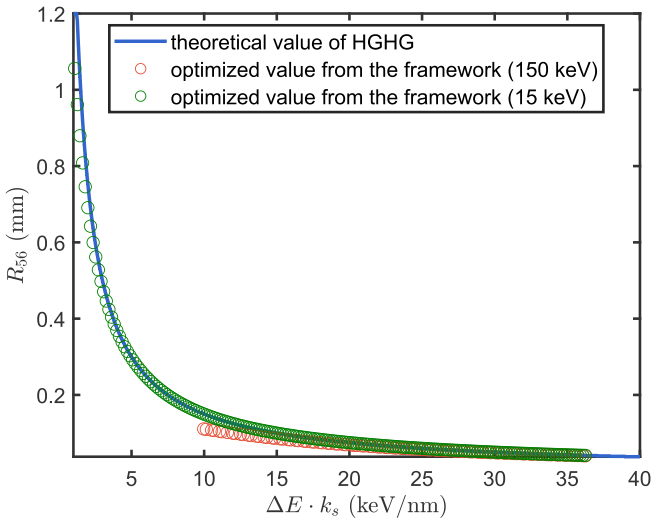



FIG. 11. Comparison of component parameters, $\Delta E \cdot k_s$ and $R_{56}$, for HGHG and the "LC" layout optimized using the optimization method. The theoretical parameter values for HGHG are indicated by the blue solid line. The optimization results are plotted as red and green dots, corresponding to initial energy spreads of 150 and 15 keV, respectively.

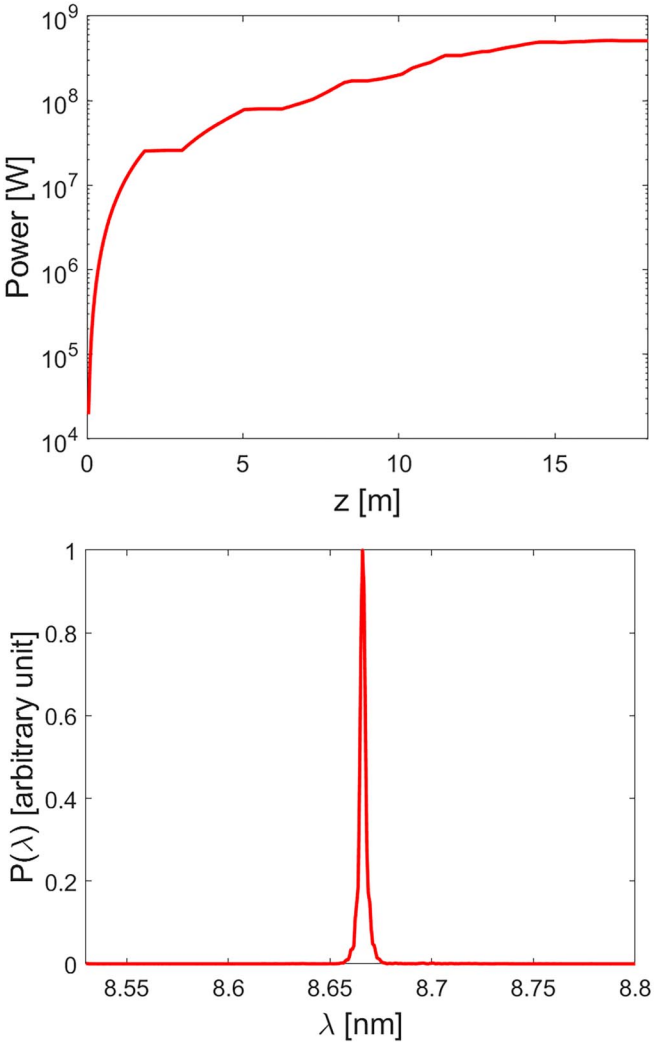



FIG. 12. FEL performance of the new scheme for the optimized solution at the 30th harmonic. Top: radiation peak power as a function of the radiator distance. Bottom: output radiation spectrum at the exit of the radiator.

In this example, the component definition module is extended with dipole and dogleg, which serve as the components for introducing transverse-longitudinal coupling. The increased number of component types leads to a significant increase in possible component layouts. As a simple demonstration using the extended component definition module, we studied a case where any layout contains no more than four components and any component type is not used more than twice. Even in this simple case, there are 284 possible layouts in total. To reduce the complexity, analogous to Example I, we excluded layouts that either lack a laser-modulator or have it positioned at the end, and consolidated consecutive dipoles or chicanes into a single component in a layout. After that, the number of possible layouts is reduced to 102.

In the optimization, the bending for both dipole and dogleg occurs only in the vertical plane. Therefore, the

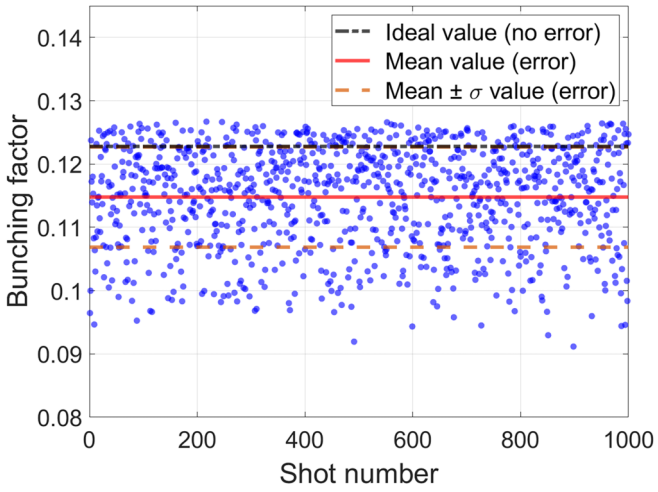



FIG. 13. Bunching factors at the 30th harmonic for 1000 shots with fluctuations in seed laser powers and magnetic fields of the chicanes for the new scheme.

beam state is simply described by the vertical and longitudinal variables $(y, y', z, \delta)$, where $y$ is the vertical coordinate, $y' = dy/dz$ is the vertical divergence, and $\delta = (E - E_0)/E_0$ is the relative energy deviation. The transport matrix of a dipole with small angle deflection is

$$R_B = \begin{pmatrix} 1 & L_B & 0 & 0 \\ 0 & 1 & 0 & -\theta_B \\ \theta_B & 0 & 1 & 0 \\ 0 & 0 & 0 & 1 \end{pmatrix}, \tag{5}$$

where $L_B$ is the length of the dipole and $\theta_B$ is its bending angle. Using the thin-lens approximation for the magnets of a dogleg, the transport matrix of the dogleg is

$$R_D = \begin{pmatrix} 1 & L_D & 0 & -L_D\theta_D \\ 0 & 1 & 0 & 0 \\ 0 & -L_D\theta_D & 1 & L_D\theta_D^2 \\ 0 & 0 & 0 & 1 \end{pmatrix}, \tag{6}$$

where $L_D$ and $\theta_D$ are its length and magnet bending angle, respectively. For the laser-modulator and chicane, the influence of $y'$ on $y$ must also be accounted for, which is different from Example I. Table III lists the ranges

TABLE II. Beam parameters of the HALF storage ring used for Example II.

| Parameter | Value | Unit |
|---|---|---|
| Energy | 2.2 | GeV |
| Rms energy spread | 1.76 | MeV |
| Vertical emittance | 10 | pm rad |
| Rms vertical size | 5 | μm |

TABLE III. Component parameter ranges for Example II.

| Parameter[a] | Min. value | Max. value | Unit |
|---|---|---|---|
| Wavelength (L) | 160 | 360 | nm |
| Modulation strength (L) | 0.088 | 17.6 | MeV |
| Phase (L) | $-\pi$ | $\pi$ | rad |
| Dispersive strength (C) | 0 | 0.1 | m |
| Length (C) | 0.15 | 10 | m |
| Bending angle (B) | −0.1 | 0.1 | rad |
| Length (B) | 0.05 | 1 | m |
| Bending angle (D) | −0.1 | 0.1 | rad |
| Length (D) | 0.1 | 5 | m |

Abbreviations: L = laser; C = chicane; B = dipole; D = dogleg.

of the parameters for all four components used in the optimization.

The final beam energy spread and bunching factor were set as the optimization objectives, and two optimizations were performed for the 15th and 30th harmonics. The coarse-to-fine optimization strategy was also adopted in the optimization. To present a clearer comparison, we merged layouts with similar microbunching principles in their optimal solutions and retained only the most representative layouts. Figure 14 presents the final optimization results and also highlights the new scheme with the "LCLC" layout.

In the case of the 15th harmonic shown in the top plot of Fig. 14, the simplest seeded FEL scheme remains HGHG with the "LC" layout, though it requires a relatively large energy spread for microbunching. In addition to the schemes with the "LCLC" layout discussed in Example I, the "BLD" scheme, corresponding to the original ADM [22], can also achieve large bunching factor at modest energy spread. However, the optimization results are inconsistent with the expected performance of the original ADM with significantly lower vertical emittance. At the 30th harmonic shown in the bottom plot of Fig. 14, the bunching factor is smaller than that of the EEHG scheme with the same final energy spread. This inconsistency is due to large vertical divergence from the relatively large vertical emittance (10 pm rad) used for the initial beam. As the vertical beam divergence increases, the transverse dispersion required for phase-merging decreases, while the longitudinal dispersion needed to rotate the merged beam's phase space remains unchanged. This leads to an increased magnet bending angle and reduced length of the dogleg.

Analysis of the optimization results reveals that the dogleg lengths in all optimized solutions with the "BLD" layout converged to approximately 0.1 m, which is the lower bound of the permitted range for the dogleg length. An increase in harmonic number reduces the required transverse dispersion. Consequently, the performance of the original ADM is further degraded. However, further shortening the dogleg length is technically challenging,

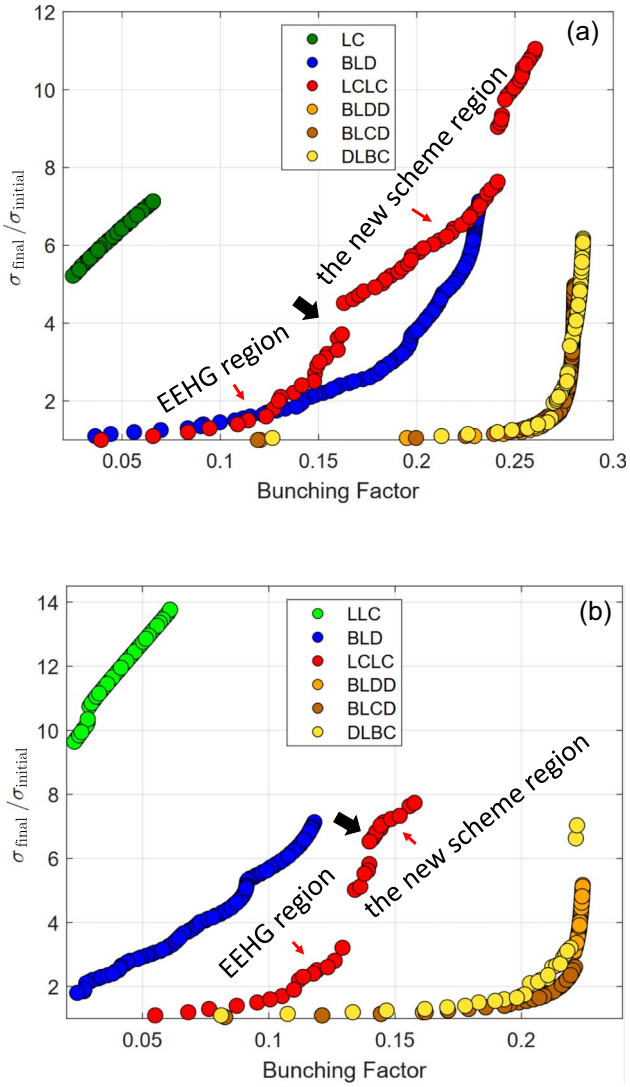



FIG. 14. Comparison of $\sigma_{final}/\sigma_{initial}$ and bunching factor at the 15th (a) and 30th (b) harmonics for the optimized solutions with different layouts in Example II, where $\sigma_{final}/\sigma_{initial}$ is the ratio of the final beam energy spread to the initial one. The position indicated by the black arrow in each plot is the inflection point representing the boundary between EEHG and the new scheme with the "LCLC" layout. The regions corresponding to EEHG and the new scheme are further indicated in each plot using text labels and red arrows.

while reducing the vertical emittance makes the intrabeam scattering effect more severe in the storage ring.

Instead, the optimization identifies viable configurations that incorporate an additional component. For example, in contrast to the original ADM scheme with the schematic layout in Fig. 15(a), the "BLDD" scheme in Fig. 15(b) adds a dogleg with an opposite bending direction at the end, which provides positive longitudinal dispersion and negative transverse dispersion. By adjusting the parameters of the two doglegs in the "BLDD" scheme, the desired longitudinal and transverse dispersions can be obtained with reasonable dogleg lengths.

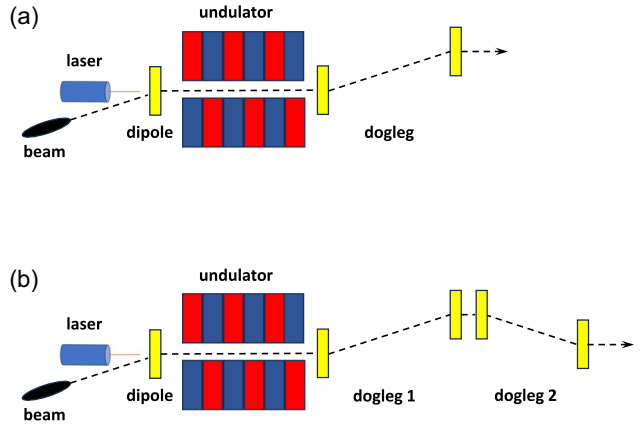



FIG. 15. Schematic layouts of the "BLD" (i.e., the original ADM) scheme (a) and the "BLDD" scheme (b). The dashed lines represent the beam path.

The final longitudinal phase spaces and current distributions of two optimized solutions for the original ADM and "BLDD" schemes are compared in Fig. 16. The two solutions are from the top plot of Fig. 14, which have the same final energy spread (approximately 1.2 times the initial energy spread). By employing an additional dogleg, the bunching factor at the 15th harmonic increases from 0.049 to 0.242, representing a significant increase by a factor of approximately 5. Besides, the optimized solutions with the "BLCD" layout, which employ an additional chicane before the dogleg, have the same function as those with the "BLDD" layout. These solutions with the "BLCD" layout are closely related to the improved ADM scheme previously proposed in Ref. [34], in which the added chicane enables independent control of the longitudinal dispersion without affecting the transverse dispersion. Figure 17 shows the longitudinal phase space evolution of two optimized solutions with the "BLDD" and "BLCD" layouts, which are from the bottom plot of Fig. 14. The two solutions have the same final energy spread, approximately 1.2 times the initial energy spread. In view of practical constraints, replacing the dogleg in the original ADM scheme is necessary for achieving better microbunching, e.g., as in the generalized longitudinal strong focusing scheme of a steady-state microbunching storage ring [35].

In Fig. 14, there is another layout, "DLBC," which has similar performance with "BLDD" and "BLCD." It had been proposed in Ref. [31]. Its physical mechanism is

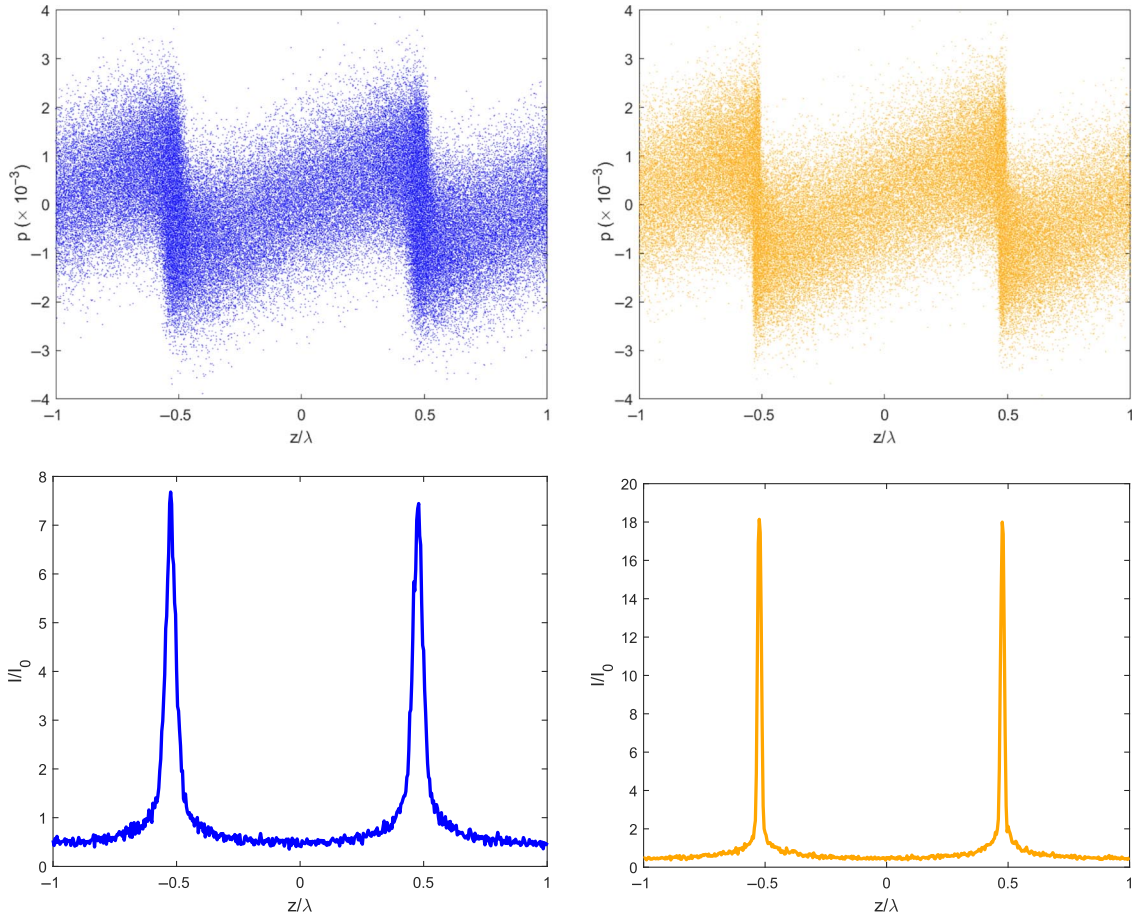



FIG. 16. Comparison of the final longitudinal phase spaces and current distributions for the original ADM scheme (left) and the "BLDD" scheme (right), obtained with the optimized solutions at the 15th harmonic.

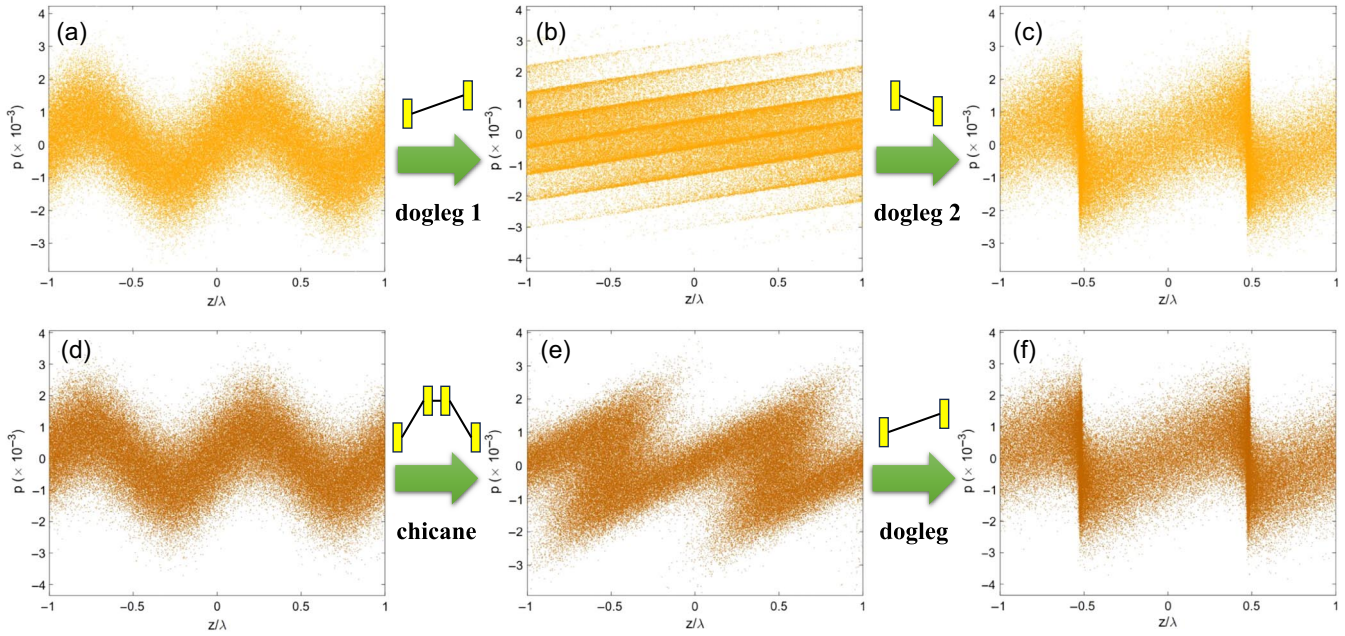



FIG. 17. Longitudinal phase space evolutions of "BLDD" and "BLCD" for two optimized solutions at the 30th harmonic. The three top plots are the longitudinal phase space distributions at the exits of laser-modulator (a), first dogleg (b), and second dogleg (c) in the "BLDD" scheme. The three bottom plots are the longitudinal phase space distributions at the exits of laser-modulator (d), chicane (e), and dogleg (f) in the "BLCD" scheme.

similar to that of PEHG but with a dipole replacing the transverse gradient undulator.

## IV. CONCLUSIONS AND OUTLOOK

In this paper, we proposed an automated optimization method for studying the microbunching in seeded FELs. The optimization is organized into five modules: component definition module, initial beam state, final beam state, objective function module, and "black box" module, each of which can be modified and extended. Utilizing components from the component definition module, the "black box" module performs numerical optimization to generate seeded FEL configurations with optimal microbunching. In the optimization, a criterion of configuration comparison was proposed to guide all solutions to develop across a wide range of harmonics and favor configurations with fewer components.

The optimization method was applied to optimize two examples. In the first example, seeded FEL configurations composed solely of laser-modulators and chicanes were investigated. The method successfully reproduced both the HGHG and EEHG schemes. It also identified a complex FEL scheme with three modulation stages, which produces some increase in bunching factor compared to EEHG. Furthermore, a new scheme with the same layout as EEHG was found, which can exhibit larger bunching factor than EEHG but at the cost of higher energy spread. A detailed analysis of the new scheme was then performed. In the second example, the components used were extended with dipoles and doglegs. The method also reproduced the results of the ADM and PEHG schemes. The original ADM may fail to achieve effective microbunching when the vertical emittance is relatively large, which is needed to suppress intrabeam scattering in an ultralow emittance storage ring. For this case, the bunching factor can be significantly increased by incorporating an additional dogleg or chicane into the original ADM, as suggested by the optimization and previous literature.

Future work will focus on applying this optimization method to a broader range of physics problems related to microbunching. One direction is to investigate more complex microbunching mechanisms involving nonlinear effects and six-dimensional transverse-longitudinal coupling. Another direction is to vary the optimization objectives to investigate different performance characteristics and trade-offs of various microbunching mechanisms. In particular, the optimization method could be used to identify configurations that reduce the required seed laser power while maintaining a sufficiently large bunching factor and other required beam properties.

## ACKNOWLEDGMENTS

We express our gratitude to Xiujie Deng of Tsinghua University for his helpful discussions.

## DATA AVAILABILITY

The data that support the findings of this article are not publicly available. The data are available from the authors upon reasonable request.

[1] D. A. G. Deacon, L. R. Elias, J. M. J. Madey, G. J. Ramian, H. A. Schwettman, and T. I. Smith, First operation of a free-electron laser, Phys. Rev. Lett. **38**, 892 (1977).

[2] C. Pellegrini, A. Marinelli, and S. Reiche, The physics of x-ray free-electron lasers, Rev. Mod. Phys. **88**, 015006 (2016).

[3] J. Duris, S. Li, T. Driver *et al.*, Tunable isolated attosecond X-ray pulses with gigawatt peak power from a free-electron laser, Nat. Photonics **14**, 30 (2020).

[4] W. Decking, S. Abeghyan, and P. Abramian, A MHz-repetition-rate hard X-ray free-electron laser driven by a superconducting linear accelerator, Nat. Photonics **14**, 391 (2020).

[5] A. Kondratenko and E. Saldin, Generating of coherent radiation by a relativistic electron beam in an ondulator, Part. Accel. **10**, 207 (1980), https://cds.cern.ch/record/1107977 .

[6] R. Bonifacio, C. Pellegrini, and L. M. Narducci, Collective instabilities and high-gain regime in a free electron laser, Opt. Commun. **50**, 373 (1984).

[7] S. V. Milton, E. Gluskin, N. D. Arnold *et al.*, Exponential gain and saturation of a self-amplified spontaneous emission free-electron laser, Science **292**, 2037 (2001).

[8] P. Emma, R. Akre, J. Arthur *et al.*, First lasing and operation of an ångstrom-wavelength free-electron laser, Nat. Photonics **4**, 641 (2010).

[9] M. Hogan, C. Pellegrini, and J. Rosenzweig, Measurements of high gain and intensity fluctuations in a self-amplified, spontaneous-emission free-electron laser, Phys. Rev. Lett. **80**, 289 (1998).

[10] E. L. Saldin, E. A. Schneidmiller, and M. V. Yurkov, Statistical properties of radiation from VUV and X-ray free electron laser, Opt. Commun. **148**, 383 (1998).

[11] L. H. Yu, M. Babzien, I. Ben-Zvi *et al.*, High-gain harmonic-generation free-electron laser, Science **289**, 932 (2000).

[12] Z. T. Zhao, D. Wang, J. H. Chen *et al.*, First lasing of an echo-enabled harmonic generation free-electron laser, Nat. Photonics **6**, 360 (2012).

[13] E. Allaria, R. Appio, L. Badano *et al.*, Highly coherent and stable pulses from the FERMI seeded free-electron laser in the extreme ultraviolet, Nat. Photonics **6**, 699 (2012).

[14] E. Allaria, D. Castronovo, P. Cinquegrana *et al.*, Two-stage seeded soft-X-ray free-electron laser, Nat. Photonics **7**, 913 (2013).

[15] E. Hemsing, M. Dunning, B. Garcia *et al.*, Echo-enabled harmonics up to the 75th order from precisely tailored electron beams, Nat. Photonics **10**, 512 (2016).

[16] L. H. Yu, Generation of intense uv radiation by subharmonically seeded single-pass free-electron lasers, Phys. Rev. A **44**, 5178 (1991).

[17] G. Stupakov, Using the beam-echo effect for generation of short-wavelength radiation, Phys. Rev. Lett. **102**, 074801 (2009).

[18] D. Xiang and G. Stupakov, Echo-enabled harmonic generation free electron laser, Phys. Rev. ST Accel. Beams **12**, 030702 (2009).

[19] P. R. Ribič, A. Abrami, L. Badano *et al.*, Coherent soft X-ray pulses from an echo-enabled harmonic generation free-electron laser, Nat. Photonics **13**, 555 (2019).

[20] H. Deng and C. Feng, Using off-resonance laser modulation for beam energy spread cooling in generation of short-wavelength radiation, Phys. Rev. Lett. **111**, 084801 (2013).

[21] C. Feng, H. Deng, D. Wang, and Z. Zhao, Phase-merging enhanced harmonic generation free-electron laser, New J. Phys. **16**, 043021 (2014).

[22] C. Feng and Z. Zhao, A storage ring based free-electron laser for generating ultrashort coherent EUV and X-ray radiation, Sci. Rep. **7**, 4724 (2017).

[23] K. Deb, A. Pratap, S. Agarwal, and T. Meyarivan, A fast and elitist multiobjective genetic algorithm: NSGA-II, IEEE Trans. Evol. Comput. **6**, 182 (2002).

[24] J. Kennedy and R. Eberhart, Particle swarm optimization, in *Proceedings of ICNN'95—International Conference on Neural Networks* (IEEE, Perth, WA, Australia, 1995), Vol. 4, pp. 1942–1948.

[25] C. A. C. Coello, G. B. Lamont, and D. A. V. Veldhuizen, *Evolutionary Algorithms for Solving Multi-Objective Problems* (Springer, Boston, MA, 2007).

[26] K. Deb, *Multi-Objective Optimisation Using Evolutionary Algorithms: An Introduction* (Springer, London, 2011).

[27] Z. Wang and Z. Bai, Optimization code for micro-bunching in seeded free-electron lasers, version 1.0.0 (2026).

[28] S. Reiche, Genesis 1.3: A fully 3D time-dependent FEL simulation code, Nucl. Instrum. Methods Phys. Res., Sect. A **429**, 243 (1999).

[29] D. Xiang and W. Wan, Generating ultrashort coherent soft X-ray radiation in storage rings using angular-modulated electron beams, Phys. Rev. Lett. **104**, 084803 (2010).

[30] Q. Jia and H. Li, Normal planar undulators doubling as transverse gradient undulators, Phys. Rev. Accel. Beams **20**, 020707 (2017).

[31] W. Liu and Y. Jiao, Generating ultrashort X-ray pulse in a diffraction-limed storage ring by phase-merging enhanced harmonic generation with normal modulator, in *Proceedings of the 9th International Particle Accelerator Conference IPAC'18* (JACoW Publishing, Vancouver, BC, Canada, 2018), pp. 1371–1374.

[32] X. J. Deng, W. H. Huang, Z. Z. Li, and C. X. Tang, Harmonic generation and bunch compression based on transverse-longitudinal coupling, Nucl. Instrum. Methods Phys. Res., Sect. A **1019**, 165859 (2021).

[33] Z. Bai, G. Feng, T. He *et al.*, Progress on the storage ring physics design of Hefei Advanced Light Facility (HALF), in *Proceedings of the 14th International Particle Accelerator Conference, IPAC'23* (JACoW Publishing, Venice, Italy, 2023), pp. 1075–1078.

[34] C. Li, B. Jiang, C. Feng *et al.*, Lattice design for an improved angular dispersion-induced microbunching scheme, J. Instrum. **17**, P11020 (2022).

[35] Z. Li, X. Deng, Z. Pan, C. Tang, and A. Chao, Generalized longitudinal strong focusing in a steady-state microbunching storage ring, Phys. Rev. Accel. Beams **26**, 110701 (2023).